Acta Cryst. (1973). A**29**, 18

Direct Observation of Lattice Defects in H-Nb_2O_5 by High Resolution Electron Microscopy

BY SUMIO IIJIMA*

Department of Physics, Arizona State University Tempe, Arizona 85281, *U.S.A.*

(*Received* 22 *May* 1972; *accepted* 11 *July* 1972)

Dedicated to Professor Tadatosi Hibi in honour of his 62nd birthday

Detailed two-dimensional lattice images, showing metal-atom positions in crystals of H-Nb_2O_5 quenched from the melt have been observed using a sophisticated electron microscope in both ordered and heavily disordered regions. The blocks in the structure were well ordered along the *b* axis, but heavily disordered in the *ac* plane; the sub-cell structure of ReO_3 was still perfectly retained. Four kinds of planar defects, oriented parallel to low-index planes in the host structure, were revealed in the ordered region. Some of these planar defects produce non-stoichiometry. A new polymorph of Nb_2O_5, having the same structure as PNb_9O_{25}, was found in one of the defect structures, and several other new phases of Nb_2O_5 were observed in the heavily disordered region. Incoherently packed blocks and unusual-size blocks played an important role as one of possible origins of the defect planes.

Introduction

The first systematic crystallographic studies of Nb_2O_5 were carried out by Brauer (1941). He found that when the powder of Nb_2O_5, produced by chemical reaction and amorphous to X-ray diffraction, was heated in air it crystallized into three kinds of structure in succession. They were called the low-temperature form, medium-temperature form and high-temperature form respectively. Subsequently, several new structures have been found for this material, chiefly by using X-ray diffraction methods. It is generally accepted that by heating the varieties to 900 °C or more in air, the high temperature form (H-Nb_2O_5) is finally obtained. Its detailed structure determination was carried out by Gatehouse & Wadsley (1965) using a single-crystal X-ray diffraction method.

It is well known that H-Nb_2O_5, whose structure is based on the ReO_3 structure, gives a family of related structures of binary oxides by reaction with other transition metal oxides in the solid state. The variation in chemical composition within a given specimen has been a main interest of many solid state chemists. It has been postulated that the non-stoichiometry of such compounds may be attributed to Wadsley defects, or intergrowth planar defects (Anderson & Wadsley, 1969).

In order to understand the non-stoichiometry and the mechanism of formation of such binary oxides structurally related to H-Nb_2O_5, it is necessary to make clear whether H-Nb_2O_5 itself is non-stoichiometric or not, and what types of defects are present.

Spyridelis, Delavignette & Amelinckx (1967) tried to make electron microscope observations of crystals of H-Nb_2O_5 and Ta_2O_5 but apparently examined only crystals of the low temperature polymorph. Allpress, Sanders & Wadsley (1969), in the course of their numerous electron microscopic observations on binary oxides, reported that they could not recognize any particular defects in crystals of H-Nb_2O_5 using thoroughly annealed samples.

Recently, with careful use of modern high resolution electron microscopy, it has been possible to show clearly the arrangement of metal atoms in a unit cell projected on the *ac* plane of the structure of $Ti_2Nb_{10}O_{29}$ (Iijima, 1971). This technique is of considerable use for the study of the nature of the defects present in such compounds which cannot be detected by X-ray diffraction techniques. The present paper concerns the electron microscopic observation, at the level of atomic resolution, of the defects deliberately formed in specimens by quenching from the melt of H-Nb_2O_5. The same sample was examined at medium resolution by Allpress (unpublished results) and many defects were observed, but because of the limited resolution, they could not be characterized in detail.

Experimental

The sample of high temperature form of Nb_2O_5 which was quenched from the melt (provided from J. G. Allpress of C.S.I.R.O., Melbourne) was ground in an agate mortar and dispersed in methyl chloroform or acetone. A copper grid with a carbon supporting film which has a number of holes of 0·1–10μ diameter was dipped in the suspension and dried. A very thin crystal edge projecting over a hole was chosen and the specimen was tilted and rotated until the crystal gave an almost symmetrical *h*0*l* diffraction pattern.

Observations were made with a JEM-100B (100 kV) microscope equipped with a goniometer stage ($\pm 30°$ tilt). A special anti-contamination device and pointed filaments were also used. In order to reduce spherical aberration and to get higher maximum magnification

* On leave from Research Institute for Scientific Measurements, Tohoku University, Sendai, Japan.

than the 3×10^5 times with the commercial goniometer specimen holder, the specimen position in the objective lens was lowered by about 1 mm, which gave a maximum magnification of $4{\cdot}2 \times 10^5$. At maximum magnification the detailed contrast in a unit cell was clearly visible on a fluorescent screen with a $10\times$ binocular microscope. The increased magnification also made it easier both to find an optimum focusing condition of the objective lens without taking a through-focal series of pictures as is usually done in high-magnification microscopy, and to check specimen drift. Exposure time was 1–3 sec at $4{\cdot}2 \times 10^5$ times. Astigmatism was corrected until negligible by obtaining homogeneous granulation in the image of the carbon film very near the specimen every time after the specimen had been set. An objective aperture of 40μ in diameter was used.

It was found in a previous experiment (Iijima, 1971) that the appearance of the two-dimensional lattice images was very dependent on the tilting angle of the crystal and on the extent of defocus of the objective lens. Required alignment was found to be within $\sim 10^{-3}$ radian and an optimum amount of defocusing was about 900 Å under-focus. The alignment of the electron beam parallel to the *b* axis is even more critical for thicker crystals.

The unit-cell structure showing metal-atom positions was observed not only in an edge region of the crystal whose thickness was less than 150 Å but also in thicker (700–1100 Å) regions. This is useful for our present purposes since we need to observe as large an area as possible even though the resolution in the images is not so good under these circumstances. A discussion of this observation will be given elsewhere.

The electron microscopic observation of crystals at high magnification is confined to a relatively small region of a crystal and will not give the same statistically averaged results as X-ray studies. Though it is desirable to examine a large number of fragments to be sure of getting representative results, the probability of coming across a suitable specimen was rather low in the present experiment (perhaps less than 0·1%). Here about 45 fragments were observed in detail at both $4{\cdot}2 \times 10^5$ and 1×10^5 times magnification.

There was no evidence that new defects were introduced into the crystals when they were ground except that some metal atoms located at the outermost surface of the crystal appeared to have been rearranged slightly. Furthermore, there was no evidence of radiation damage during the observation.

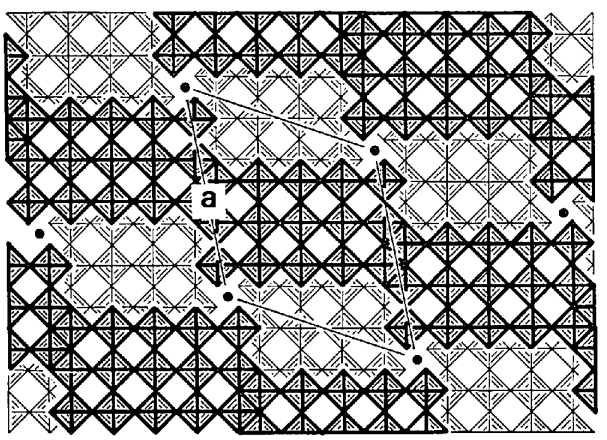

(*a*)

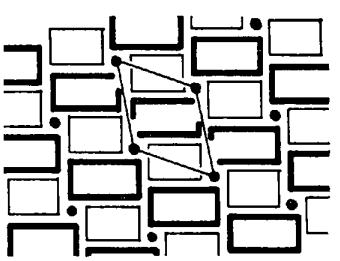

(*b*)

Fig. 1. (*a*) Idealized model of the structure of *H*-Nb_2O_5 and (*b*) its simple representation. The darker and lighter squares which form 3×5 and 3×4 blocks by their corner sharing are centred about the two levels perpendicular to the *b* axis and are 1·9 Å apart. The black circles represent the tetrahedrally coordinated Nb atoms. The unit cell is outlined (a=21·2 Å, b=3·8, c=19·4 Å and β=120°).

Interpretation of lattice images

Since our two-dimensional lattice images, taken under the above-mentioned conditions, were recorded with many beams included in the objective aperture, the interpretation of their image contrast can be done using *n*-beam dynamical theory and has been already discussed in some detail (Cowley & Iijima, 1972). When the specimen is thin enough to be considered as a phase object, maximum contrast of the image will be obtained at a slightly under-focused condition and linearly proportional to the projected potential distribution of the crystal along the beam direction. This is known as the 'optimum defocus condition' for imaging of a phase object as proposed by Scherzer (1949) and others (Heidenreich & Hamming, 1965; Erickson & Klug, 1970).

For the present case, where crystals have thicknesses of the order of 100 Å and contain relatively heavy atoms, the phase-object approximation, which may be valid for biological materials consisting of light atoms (Grinton & Cowley, 1971), is inadequate to explain the detailed image intensity of photographs of complex niobium oxides.

A modified theory for the phase-object approximation involving large phase changes of the electron wave shows that the contrast in the image of an isolated peak of potential projected along the incident beam direction will be almost independent of the peak height but will depend only on the width of the peak (Cowley & Iijima, 1972). When we derive complicated structural defects from their abnormal image contrasts, the modi-

fied interpretation must be used. For our present purpose however, it can be said that the distribution of the contrast in the image corresponds roughly to the projection of the structure onto the *ac* plane of the crystal.

Results

Fig. 1(*a*) and (*b*) shows an idealized model of the H-Nb_2O_5 structure projected onto the *ac* plane along the short *b* axis (Gatehouse & Wadsley, 1965) and its simple representation. Each square represents an octahedron of a simple rhenium trioxide structure. Two kinds of blocks, shown by dark and light squares, are centred about the two levels perpendicular to the *b* axis and are 1·9 Å apart. At one level, the blocks have the dimensions 3 wide × 5 long, and are joined by octahedral edge sharing, to form separated, stepped rows. At the other level the blocks are 3 wide × 4 long, and are separated by Nb atoms in tetrahedral sites. The 3 × 4 and 3 × 5 blocks are joined by sharing their common edges which form crystallographic shear planes. The unit cell (outlined in the models) has the dimensions $a=21{\cdot}16$, $b=3{\cdot}822$, $c=19{\cdot}35$ Å and $\beta=119{\cdot}8°$.

A typical two-dimensional lattice image of H-Nb_2O_5 looking down the short *b* axis [for instance, Fig. 17(*a*)] shows a contrast distribution very similar to the *ac*-plane projection of the structure of the crystal. The channels containing no niobium atoms are imaged as white dots, the regions where octahedra share their edges, or shear planes, show grey contrast and the region near tetrahedrally coordinated metal atoms surrounded with eight metal atoms in the nearest octahedra are black.

Fragments which were examined could be classified into two groups; those which showed a well ordered block structure of H-Nb_2O_5, and the heavily disordered regions for which the arrangements of the blocks of the host structure were almost unrecognizable. About 15% of 45 fragments examined here showed the latter arrangements of the blocks. The degree of ordering of the blocks changed from fragment to fragment, as should be expected from an unannealed specimen, quenched from above the melting point.

In the first section, observations on relatively well ordered regions of H-Nb_2O_5 will be described, and in the second section, those on heavily disordered regions.

1. *Defects in an ordered region*

Fig. 2 shows a low magnification image of a relatively well ordered region in a fragment of the quenched H-Nb_2O_5 which contains several typical examples of defects. The image was taken along the *b*-axis direction of the crystal, so that it shows the *ac* plane of the structure of H-Nb_2O_5. All following photographs were taken under the same conditions. The image contains contrast having the two-dimensional lattice periodicity of the host structure, but in addition, there are a number of dark lines or bands in several different directions. Their contrast distributions are distinctive. Generally, these defect lines and bands are classified into four groups, having orientations which are parallel to the *c* axis, to the [101] direction, to [10$\bar{1}$] and to the *a* axis (labelled in the image by *A*, *B*, *C* and *D* respectively). It is of interest that they never disappear within the crystal except when they intersect other faults or the crystal edge. Their terminal structures will be discussed in connection with their growth mechanism in § 3.

(*a*) *Planar defects parallel to the c axis* (*type A*)

Fig. 3 shows a high magnification image of the defects labelled *A* in Fig. 2 and an inset represents the block model corresponding to the enclosed area. The structure of H-Nb_2O_5 can be expressed as a sequence of rows of *A* and *B* as shown in the model (Allpress & Wadsley, 1969). *A* is a row of the 3 × 4 blocks. The defects, therefore, can be expressed as a sequence of –*A*–*B*–*A*–*A*–*B*–*A*–, where two rows of *A* adjoin in the sequence (giving rise to *super*-stoichiometry). A similar type of the defect expressed by the sequence –*B*–*A*–*A*–*A*–*B*– was rarely observed (indicated by big arrow in Fig. 9). The structure expressed by a sequence of –*A*–*A*–*A*–*A*–, composed of only the 3 × 4 blocks, will correspond to the structure of $WNb_{12}O_{33}$ which is known as one of the oxidation structures of H-Nb_2O_5 (Roth & Wadsley, 1965). The fact that the outline of each of the blocks in a faulted region is very distinct, as in the host structure, indicates that they are stacked through the crystal along the *b* axis, so that those defects are two-dimensional planar defects parallel to the *b* and *c* planes (perpendicular to the paper). Therefore they can be regarded as a kind of stacking fault. The displacement in the lattice planes parallel to the *a* axis (1·9 Å, estimated from model) occurs across the defect plane.

The defects frequently appear in groups at intervals of 2*a* or 3*a*. Fig. 4(*a*) shows an example of a periodical appearance of the defect (interval of 3*a*) in the matrix of the H-Nb_2O_5. It can be seen that the faulted region forms a superlattice containing six unit cells of H-Nb_2O_5. The unit cell represented in Fig. 4(*b*) has dimensions of $a=157{\cdot}8$, $b=3{\cdot}8$, $c=19{\cdot}4$ Å and $\beta=121°$. The composition is $Nb_{97}O_{234}$. The general formula for such a superlattice structure is expressed by $Nb_{28n+13}O_{70n+33}$, where n is the number of unit cells of H-Nb_2O_5 between two defects of type *A*. The electron diffraction pattern shown as inset from this fragment shows splitting of the spots by about $\frac{1}{7}$ [100] along the a^* axis which is obviously caused by an occurrence of this superlattice. Generally the fragments containing these defects randomly arranged give an electron diffraction pattern with streaks along the [100] reciprocal-lattice direction.

Most of these defects are straight but sometimes they are dislocated or curved and broadened as shown in Fig. 5(*a*). The unusual black dots in an overlapping region of the two defect planes can be explained by considerations similar to those given by Allpress (1970), in which the displacement of a shear plane perpendic-

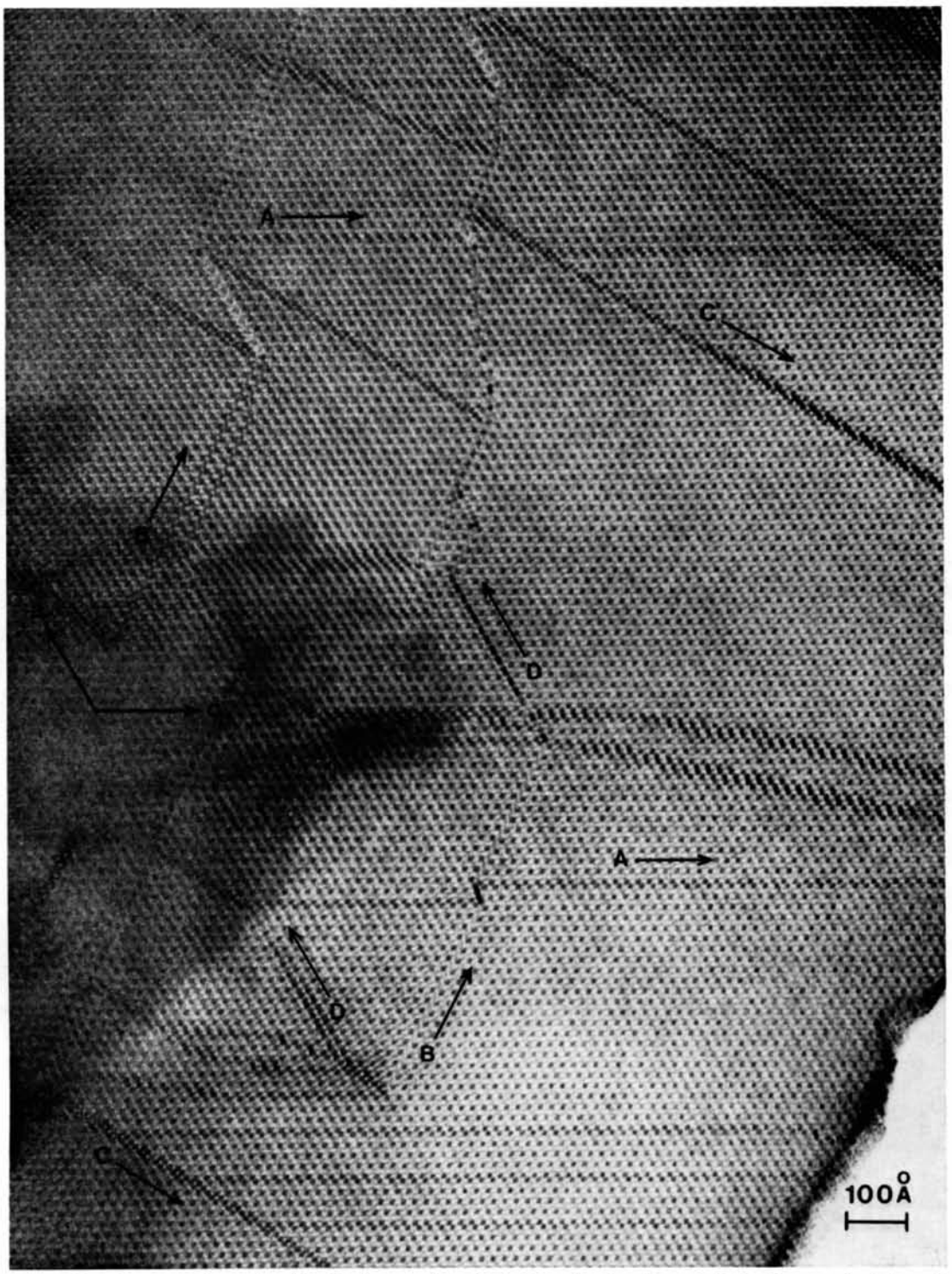

Fig. 2. Low magnification, two-dimensional lattice image of a relatively ordered region of H-Nb_2O_5 quenched from the melt, viewed down the b axis, showing four kinds of planar defects labelled A, B, C and D.

[To face p. 20

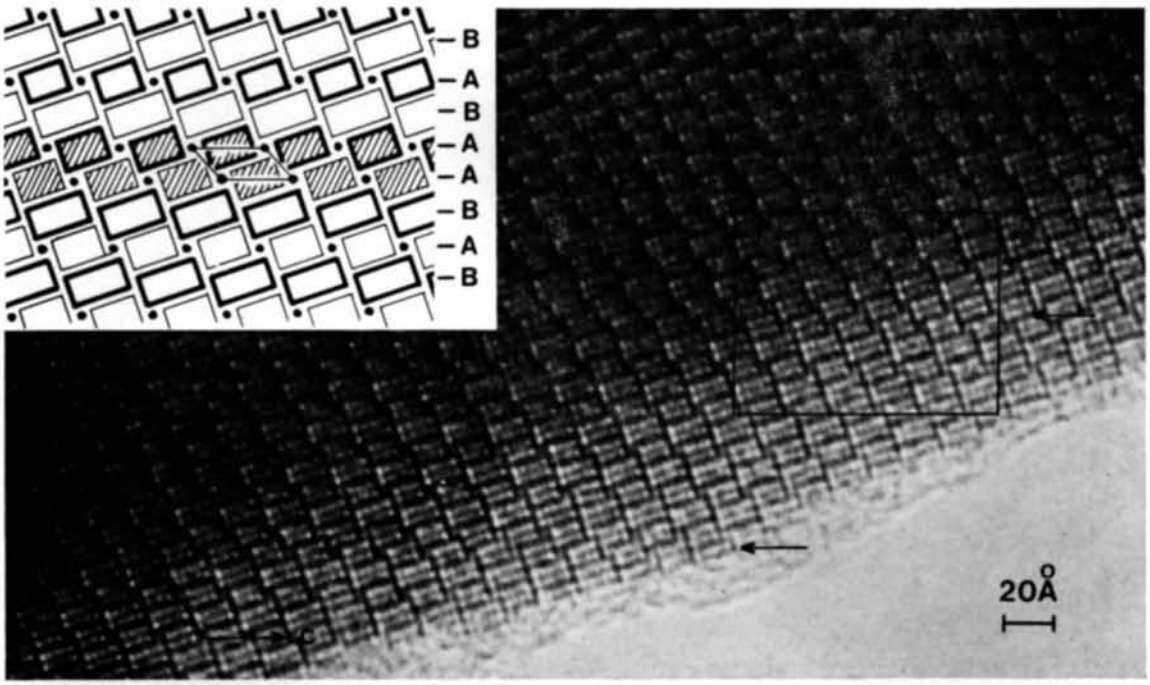

Fig. 3. Two-dimensional lattice image of H-Nb_2O_5 showing defects of type A parallel to the c axis. Inset corresponds to the enclosed area.

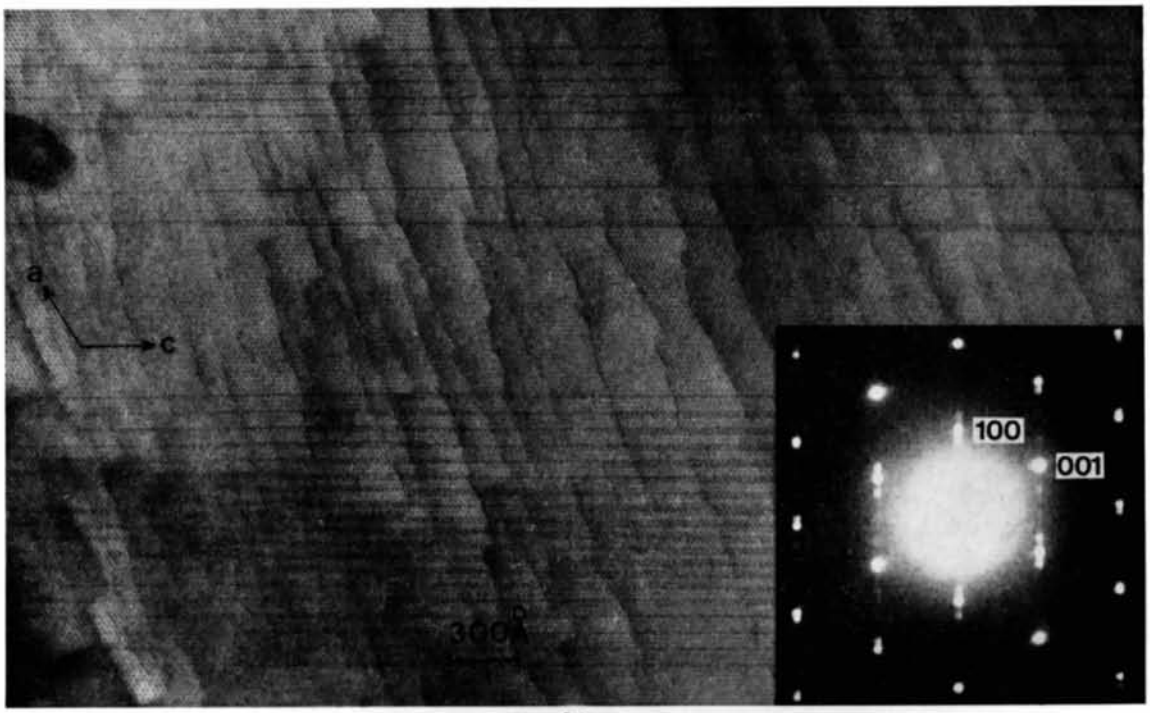

(*a*)

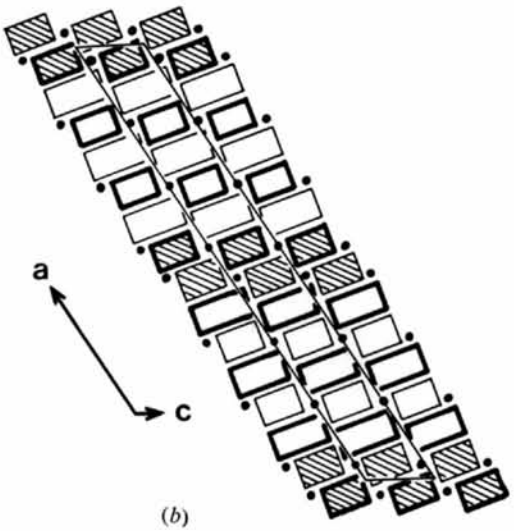

(*b*)

Fig. 4. (*a*) Low magnification two-dimensional lattice image showing a superlattice produced by a periodical arrangement of defects of type *A* in the matrix. Electron diffraction pattern (inset) of the crystal imaged shows the splitting of the spots due to the superlattice structure. Model shown in (*b*) represents the unit cell of the superlattice which has the dimensions $a = 167{\cdot}8$, $b = 3{\cdot}8$, $c = 19{\cdot}4$ Å and $\beta = 121°$.

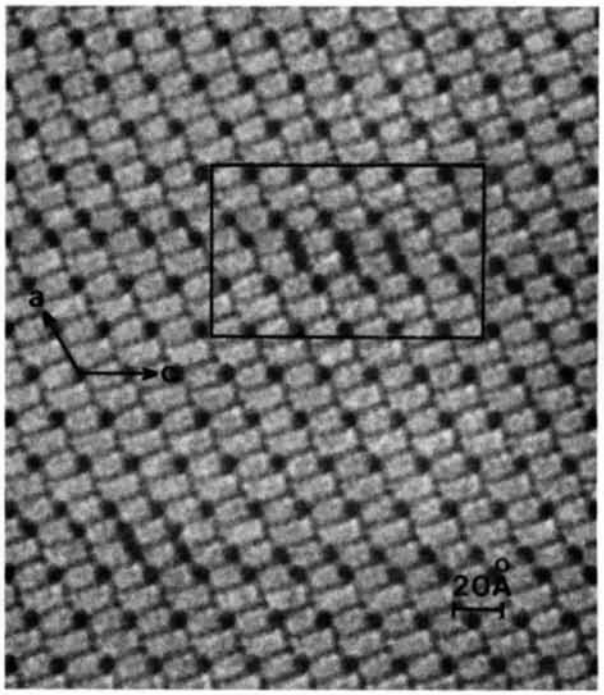

(*a*)

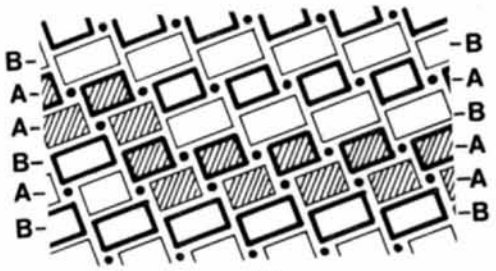

(*b*)

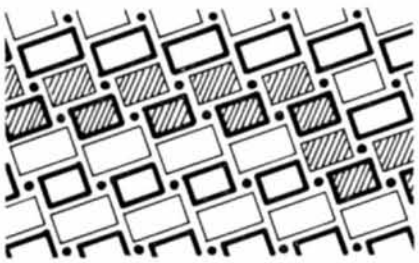

(*c*)

Fig. 5. (*a*) Two-dimensional lattice image showing a displacement of the defect of type *A* along the *a* axis by a lattice translation vector **a**(=21·16 Å) and perpendicular to the *b* axis. Unusual black dots in the overlapping region of the two defects can be explained by a superposition of the two different arrangements of the blocks shown in (*b*) and (*c*).

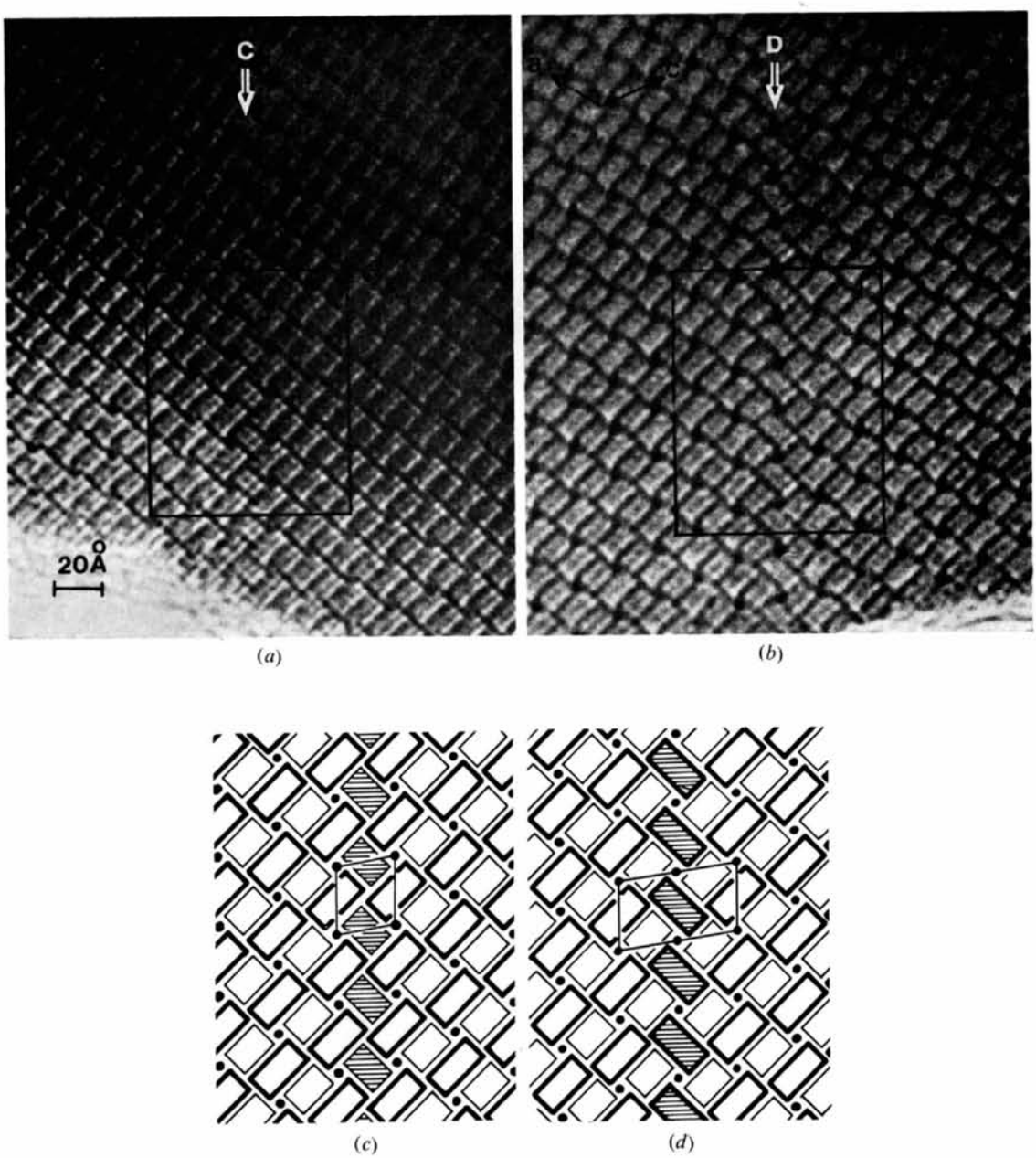

Fig. 6. Two-dimensional lattice images showing two types of defects of type *B*, or sub-twin structures, parallel to the [101] direction which are composed of 3×4 blocks (*a*) and 3×5 (*b*) and their models ,(*c*) and (*d*).

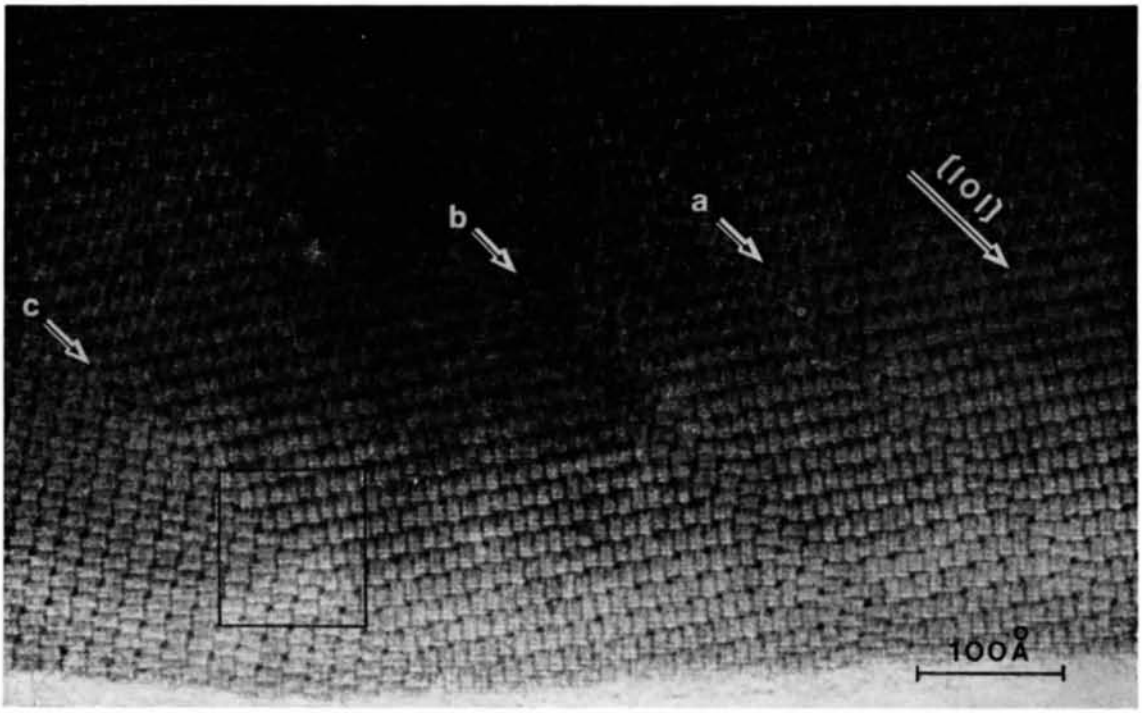

(*a*)

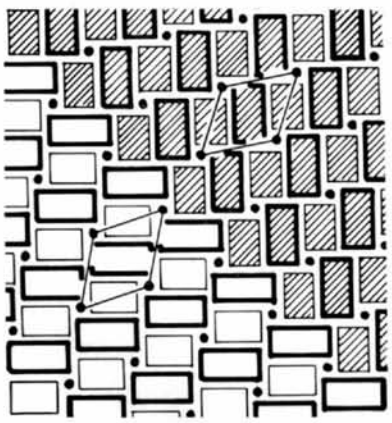

(*b*)

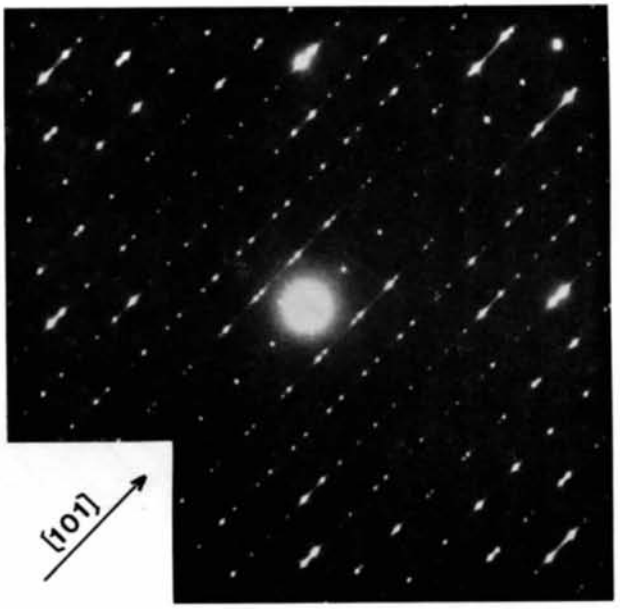

(*c*)

Fig. 7. (*a*) Two-dimensional lattice image showing micro-twin bands *a*, *b* and a twin boundary *c*. (*b*) Model representing the arrangement of blocks at the twin boundary corresponding to the enclosed area in the image. (*c*) Electron diffraction pattern from the crystal imaged in (*a*) showing the twin spots and the streaks along the [101] direction due to the micro-twin bands.

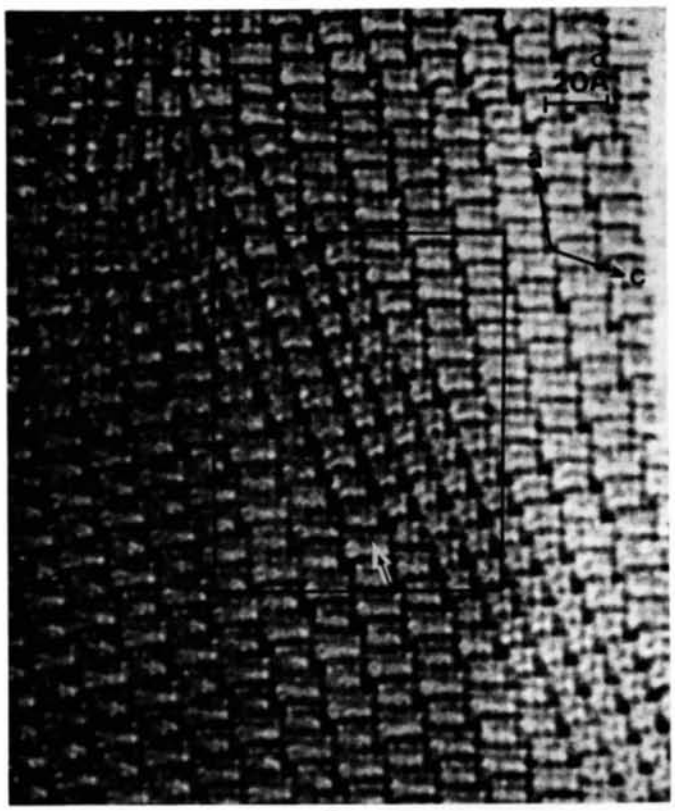

(a)

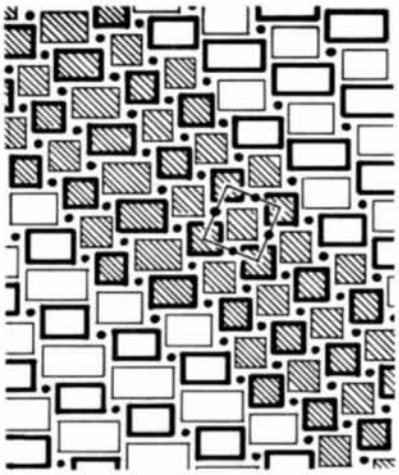

(b)

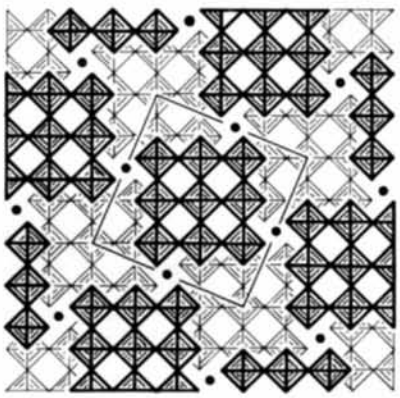

(d)

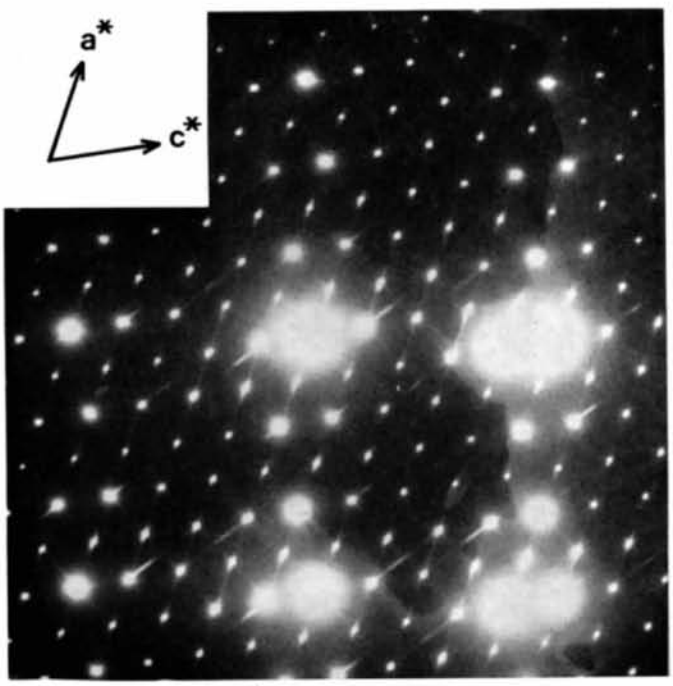

(c)

Fig. 8. (*a*) Two-dimensional lattice image showing the defect of type *C* parallel to the [10$\bar{1}$] direction, which has the same structure as PNb_9O_{25}, composed of only 3×3 blocks and (*b*) its model. (*c*) Electron diffraction pattern from the crystal imaged in (*a*) showing the streaks along the [101] direction whose maximum-intensity positions can be indexed to be from the tetragonal structure in the defect band. (*d*) Idealized model representing the structure of PNb_9O_{25}.

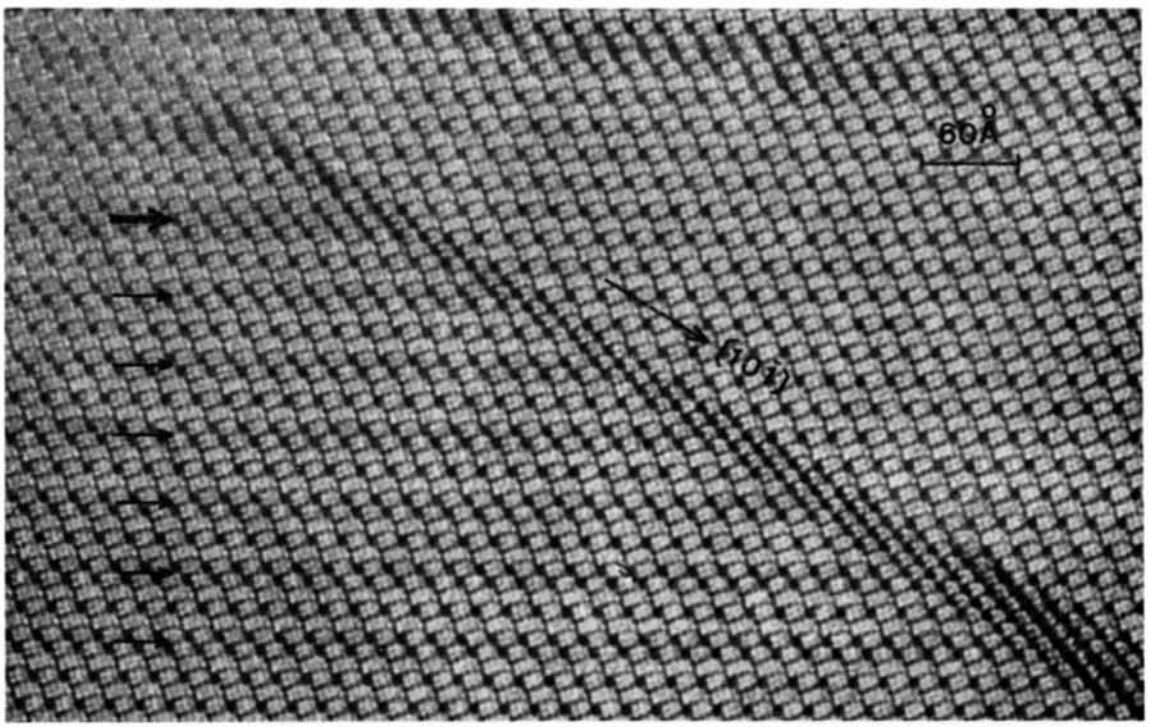

Fig. 9. Two-dimensional lattice image showing an interaction between the defects of type *A* and *C*.

[*To face p.* 21

ular to the *b* axis gives an unusually high contrast. In this case, the contrast can be explained reasonably by a superposition of the two different arrangements of the blocks shown in Fig. 5(*b*) and (*c*) which corresponds to the enclosed area. From this model, a sequence of *–B–A–B–A–A–B–* at the right hand side of the photograph is changed into *–B–A–A–B–A–B–* at the left. The fault plane, therefore, is displaced by a lattice translation vector **a** (=21·16 Å). Successive occurrence of such a displacement in the defect makes it appear bent. These defect planes usually originate from (or terminate on) other defect planes of type *C* as will be described later.

The niobium–oxygen ratio O/M of the outlined unit structure in the defect band shown in Fig. 3 is 2·538. This type of defect was observed so frequently that its density must be much higher than that of the other defects. These defects will therefore modify the composition to give a *greater* metal–oxygen ratio than in Nb_2O_5.

(*b*) *Microtwin bands parallel to* [101] *direction* (*type B*)

Fig. 6(*a*) and (*c*) shows a high magnification image of the defects labelled *B* in Fig. 2 and the block model of the outlined region. The defect consists of a row of the 3×4 blocks (*C*) parallel to the [101] direction. The longer sides of the 3×4 blocks of this extra row are rotated by 90 degrees with respect to those in the host lattice (we shall call this type of block, *V*-type). From the same considerations as in § 1(*a*), this defect is also extended two-dimensionally parallel to the *b* axis and the [101] direction of the structure. This defect produces a shift of the arrays of tetrahedral positions along the [001] direction, or the (100) plane, by 4·9 Å at the boundary. However, this does not involve any change in the periodicity of the (001) plane (spacing, 15·4 Å). In other words, when the crystal is imaged with the incident beam parallel to the (101) plane, this type of defect generally would not be detected in its one-dimensional lattice image.

Fig. 6(*b*) and (*d*) shows an image and model of the same type of defect except that a row of the *V*-type 3×4 blocks, (*C*) in Fig. 6(*a*), is replaced with that of *V*-type 3×5 blocks (*D*). The (100) planes are displaced at the boundary by 9·8 Å but there is no change in the periodical appearance of the arrays of tetrahedral positions along the [100] direction, as in the previous case.

It is of interest that the chemical composition of the unit structure (enclosed in the models) in the faulted region, is the same as that of Nb_2O_5 in both cases. These types of defect therefore make no contribution to any deviation from stoichiometry of *H*-Nb_2O_5.

Similar types of defect planes (or bands) expressed as combinations of the two types of defect *–D–C–* and *–D–C–D–C–* can be seen in Fig. 7(*a*) (indicated by *a* and *b*). At the left hand side of the boundary shown as *c*, the orientation of all blocks is changed into that of the *V*-type blocks. A model of the boundary corresponding to the enclosed area in the image is illustrated in Fig. 7(*b*) where unit cells are outlined in both regions. It is obvious that this is a twin boundary. This is confirmed from the electron diffraction pattern taken from the region of the boundary shown in Fig. 7(*c*), where two kinds of diffraction spots due to two differently oriented *H*-Nb_2O_5 phases are in mirror symmetry with respect to their common [101] axes and their two a^* axes make 120° with each other as expected from the image. The streaks of the diffraction spots parallel to the [101] direction come from the defect planes *C*, *D* and their combinations in the crystal.

A single row of *C* or *D* is the smallest unit of twinning (less than one unit cell) in this structure, so that it will be better to call it a sub-twin. These microtwins which often occur in heavily disordered regions will be discussed again later.

(*c*) *Defect band consisting of* 3×3 *blocks* (*type C*)

Fig. 8(*a*) and (*b*) shows a high-magnification image of the defects oriented in the [10$\bar{1}$] direction labelled *C* in Fig. 2 and a model corresponding to the enclosed area in the image. It is quite obvious that the fault band is composed of only 3×3 blocks which are combined with four tetrahedral positions at their corners. Near the end of this defect plane, there is an unusual 3×6 block (encircled) which will be discussed in connection with the origin of the fault planes in § 3.

Fig. 8(*c*) shows an electron diffraction pattern from this fragment. In addition to the streaks along the [100] direction which are caused by the presence of defect planes of type *A*, there are strong streaks along the [101] direction of the host structure which corresponds to the direction of the normal to the defect bands. Consequently these streaks are related to the collection of defects of type *C*. The peak positions of the maximum intensity of the streaks could be indexed to be from a tetragonal structure with unit-cell dimensions $a=c=15{\cdot}3$ Å [indicated in the model, Fig. 8(*d*)]. This structure is the same as that of PNb_9O_{25} observed by Roth, Wadsley & Anderson (1965) whose model is represented in Fig. 8(*d*). This has been expected to be a polymorph of Nb_2O_5 (Andersson & Wadsley, 1969).

Sometimes these fault bands contained an irregularity (indicated by an arrow in the image) where a row of 3×3 blocks is replaced by a row of 3×4 blocks. The periodicity of the arrangement of the blocks in the defect is interrupted by this extra row and a step is formed on the boundary. Consequently defect bands containing such extra rows of 3×4 blocks will not be straight.

Fig. 9 shows the image of an interaction between this defect and the defects of type *A* (indicated by arrows). Near the end of the defect of type *C* (upper left) there are many displacements of the shear planes perpendicular to the *b* axis as described in § 1(*a*) and more 3×3 blocks are formed in the region where several defects of type *A* terminate. A PNb_9O_{25} type structure of Nb_2O_5 is established after the bunch of defects of type *A* intersect the defect band. It can be seen that the de-

fect band can be widened by meeting a defect of type *A*. This gives rise to a variation of their widths from 10 to 100 Å.

Here again, the structure of these defect bands (PNb_9O_{25} type) is one of the family of Nb_2O_5 structures, so that the stoichiometric composition of the crystal is retained.

(*d*) *Planar defects parallel to the a axis (type D)*

Several different kinds of planar defects parallel to the *a* and *b* axes were observed. Fig. 10(*a*) and (*b*) shows an image of the most common defect in this category (indicated by arrows) and its block model corresponding to the enclosed area in the image which consists of a row of 3×5 blocks parallel to the *a* axis. The width of this defect plane is slightly greater (by 1·6 Å) than the (001) spacing (15·7 Å) and the difference seems to be difficult to detect in one-dimensional (001) lattice fringes. However the larger displacement in the lattice planes parallel to the *c* axis (9·2 Å) occurs across the defect plane. It should be noted that this defect slab disappears at the position where the different defect plane of type *A* meets it.

Fig. 11(*a*) shows a high magnification image of a defect having abnormal black contrast which consists of two parts, shown by *A* and *B*. Near the connection of the two defects, a defect plane of type *A* traverses the defect. The part between two parallel 3×4 blocks in the faults (*A*) gives strong contrast alternately. As mentioned in § 1(*a*), this contrast can be reasonably explained by assuming the superposition of two different arrangements of blocks along the *b* axis shown in Fig. 11(*b*) and (*c*). In order to realize the model, there are two possible ways of packing the blocks along the *b* axis as shown in Fig. 11(*d*) and (*e*). By taking into account the relationship with the other defect (*B*), the former model seems to be the more probable arrangement of the blocks in this case, with 3×4 and 3×5 blocks stacked alternately along the *b* axis.

By a similar consideration, the detailed contrast of defect (*B*) can also be explained by the model suggested by Allpress (1970). Suppose the whole defect plane (*A*) was displaced perpendicular to the *b* axis in the [001] direction by a lattice translation vector **c** (= 19·3 Å), somewhere near the middle of the specimen. The distribution of the black band of the defect is in quite good agreement with the high density region of the metal atom positions in the *ac*-plane projection as shown in Fig. 11(*f*) which corresponds to the enclosed area *B* in the image. The three-dimensional model of this defect obtained from these results is shown in Fig. 11(*g*).

Here it should be noted that the black contrast in the defect band does not necessarily correspond to a high atomic density region in the crystal. The metal–oxygen ratio of the defect band (*A*) was estimated to be O/M = 2·82 from the model, which was larger than the 2·5 of the host structure of H-Nb_2O_5. However since the number of the defects of type *D* is much smaller than the other three types of defects, this would not be an effective source of non-stoichiometry.

2. *Heavily disordered region*

Fig. 12 shows an image of the typical example of a heavily disordered region of a quenched fragment of H–Nb_2O_5 also viewed down the *b* axis. Various sizes of blocks 3×3, 3×4, 3×5, 3×6, 4×4 and 4×5 are packed coherently (by octahedra-edge sharing) but in disordered manner in the *ac* plane. The fact that each block shape is still clearly distinguishable except for the region showing the abnormal black contrast, indicates that the ordering of the blocks along the *b* axis is well retained despite heavily disordered arrangement of the blocks in the *ac* plane. An area of regularly arranged tetrahedral positions can be seen in the bottom of the image. These are obviously similar to the micro-twin bands as described in § 1(*b*) which are parallel to the [101] direction. This type of ordering can also occur even in a very small area as indicated by circle *A*.

The abnormal black contrast in the central region of the image could be reasonably explained by assuming displacement of the blocks perpendicular to the *b* axis according to similar considerations described in § 1(*d*). For instance, Fig. 13(*a*) shows an enlargement of the area outlined by circle *B* in Fig. 12. The black contrast region is in good agreement with the higher density region in the *ac*-plane projection of metal-atom positions, which is obtained by superposing two different arrangements of the blocks shown in Fig. 13(*b*) and (*c*).

Let us examine some of the locally ordered structures which often occur in a heavily disordered region of the crystal. The enclosed region shown in Fig. 14(*a*) has an ordered structure which can be described as a periodical occurrence of rows of *V*-type 3×5 blocks [labelled *D* in Fig. 6(*b*)] in the host structure of H-Nb_2O_5. The unit cell shown in the model in Fig. 14(*b*) has the dimensions about $a=19$, $b=3{\cdot}8$, $c=32$ Å and $\beta=80°$, and is exactly the same as the sub-twin structure shown in Fig. 6(*d*). In another words, this structure can be regarded as regularly ordered multiple sub-twin bands. Therefore the periodicity in the arrays of tetrahedral positions along the [101] direction of the host lattice is still retained. The chemical composition of this structure is Nb_2O_5 ($Nb_{56}O_{140}$) so that it may be regarded as one of the possible polymorphs of Nb_2O_5, and such an ordered defect does not affect the stoichiometry of the crystal.

A similar structure can be seen in Fig. 15(*a*) (enclosed by square *A*). The unit cell shown in Fig. 15(*b*) whose dimensions are $a=19$, $b=3{\cdot}8$, $c=16$ Å and $\beta=99°$, corresponds to another sub-twin structure shown in Fig. 6(*a*). This structure also has the same composition, Nb_2O_5 ($Nb_{28}O_{70}$), as H-Nb_2O_5. In this image there is another ordered structure (enclosed by square *B*) which is the orthorhombic modification of N-Nb_2O_5 consisting of only 4×4 blocks whose monoclinic phase has been reported as one of the polymorphs of Nb_2O_5 by Andersson (1967). The unit cell

shown in Fig. 15(*c*) has the dimensions $a=c=28{\cdot}5$, $b=3{\cdot}8$ Å.

It may be said, intuitively, from the examples mentioned above that even a heavily disordered region has a tendency to have the same chemical composition as the parent ordered structure of H-Nb_2O_5.

3. *Origin of defect planes*

As mentioned in § 1, defect planes often intersect and sometimes terminate (or originate) at the point of intersection. It is of interest to examine the end structures of the defect planes to determine how they originate or terminate. Fig. 16(*a*) and (*b*) shows an image of a termination of two defects planes of types *B* and *C* and an octahedral model of the outlined area. It is clear that there are three unusual blocks near the apex formed by the two defect planes, where two blocks lying on the same level in the *ac* plane are combined. It was found that these joining blocks are still composed of niobium–oxygen octahedra with octahedra-corner and -edge sharing. Similar unusual blocks were frequently observed at the intersections of two or more defect planes [for instance, 3×6 blocks are situated at the point of intersection of the defect planes in Figs. 8(*a*) and 10(*a*)].

These examples indicate evidently that these unusual blocks are related to the presence of the defect planes. However, it will be difficult from these photographs to determine whether these blocks nucleate the defects or whether they result from the strain produced by interaction of the defect planes.

Another example of the terminal structure of defects is shown in Fig. 17(*a*) where unusual blocks are also present. The longer sides of two adjacent 3×5 blocks (enclosed by circle) are not parallel. From these blocks the defect of type *B* and a planar defect parallel to the *a* axis are extended. Fig. 17(*b*) shows a possible octahedral model of the outlined area. It was found that in the latter defect plane the packing of blocks is still coherent except for near the encircled area but the 3×5 blocks are slightly distorted from the rectangular shape and the former tetrahedral positions seem to be occupied by two metal atoms, probably with an associated rearrangement of the surrounding anion positions. Furthermore the *ac* plane is dislocated by a lattice vector **b** (3·8 Å) across the defect as shown in Fig. 17(*c*). Therefore the encircled area is very similar to a screw dislocation.

From this picture it may be possible to speculate on the growth of the defect planes. The two deformed 3×5 blocks will probably act as a nucleus for the two defect planes, with the divergence of the longer sides of the blocks probably caused by the presence of impurity atoms because of the difference in metal–oxygen bonding length. Once distortedblocks are formed in a homogeneous host structure, the surrounding strain is accommodated by a proper local rearrangement of blocks (usually by accompanying different sized blocks). Finally a metastable arrangement of blocks, which will be a defect plane, is accomplished, and will continue to grow in the same direction. Consequently the solidification of the crystal in this case seems to have taken place along a direction near to the [201] direction.

Discussion

The crystals of H-Nb_2O_5, based on ReO_3 structure, are particularly suitable for this type of study. In order to resolve two adjacent potential peaks of metal atoms (actually they correspond to two linear arrays of up to about 50 metal atoms in the present case), the distance between the two peaks should be larger than the resolution of the electron microscope (Cowley & Iijima, 1972). The distance between two adjacent metal atoms in the ReO_3 structure projected onto the principle planes (3·8 Å) is comparable with the resolution of 3 to 4 Å of our modified electron microscope so that it is possible to resolve metal-atom positions in the unit cell of the crystal. This will apply to other types of structures if metal atoms are separated enough to satisfy the above condition, as in the tetragonal tungsten bronze type structure of the Nb_2O_5–WO_3 system (Iijima, to be published).

Since the image contrast is very dependent on focusing of the objective lens, it will not be easy to pick up a 'true image', corresponding to a projected structure of the crystal, among a series of photographs without any pre-knowledge about the crystal concerned. However it may be possible to take a 'true image' from any unknown crystal once the so called 'optimum defocus condition' has been found for a given electron microscope because it is determined by instrumental factors only. In practice, it is important that one of three axes of a unit cell should be considerably smaller than the others to allow a suitable fragment having a desired orientation to be chosen from among randomly scattered fragments and also materials should be stable under the intense electron irradiation which is inevitably required for observation at extremely high magnification.

In H-Nb_2O_5, almost all blocks are arranged coherently even in a heavily disordered region of the crystal and also they are well ordered along the short *b* axis. This indicates that metal–oxygen octahedra in the blocks of ReO_3 structure tend to join to others by octahedra-edge sharing, even in the boundary between a defect and a host structure, without appreciable lattice distortion. The better ordering along the *b* axis of H-Nb_2O_5 may be related to the extremely high diffusion rate of oxygen along the *b* axis in this kind of crystal (Sheasby & Cox, 1968). This also will be a reason why only two-dimensional defect planes parallel to the *b* axis are formed so often. Such a high anisotropy in crystal growth seems to prevent the occurrence of the dislocations in this crystal.

Since almost all blocks were ordered along the *b* axis even in a disordered region in the *ac* plane, it is possible, in principle, to determine the chemical composition of the crystal by counting metal-atom positions in

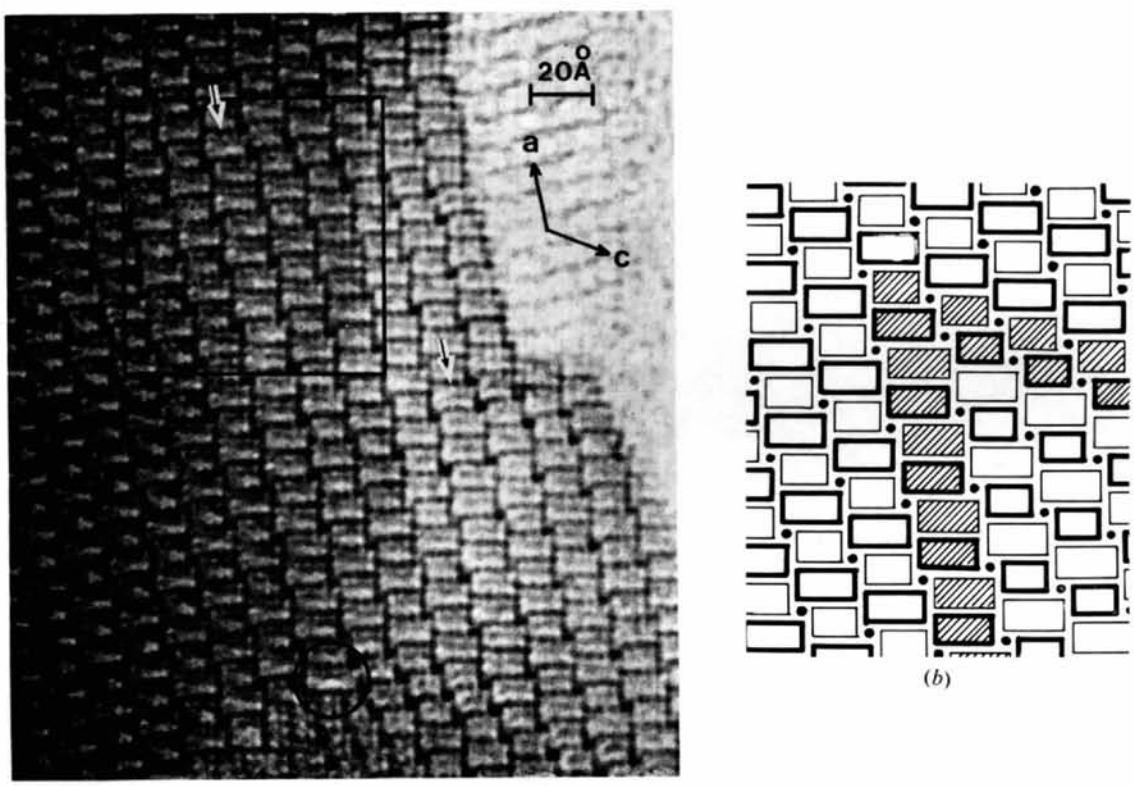

(a) (b)

Fig. 10. (*a*) Two-dimensional lattice image showing the defect of type *D* parallel to the [100] direction which disappears by meeting the defect of type *A*, and (*b*), its model.

To face p. 24

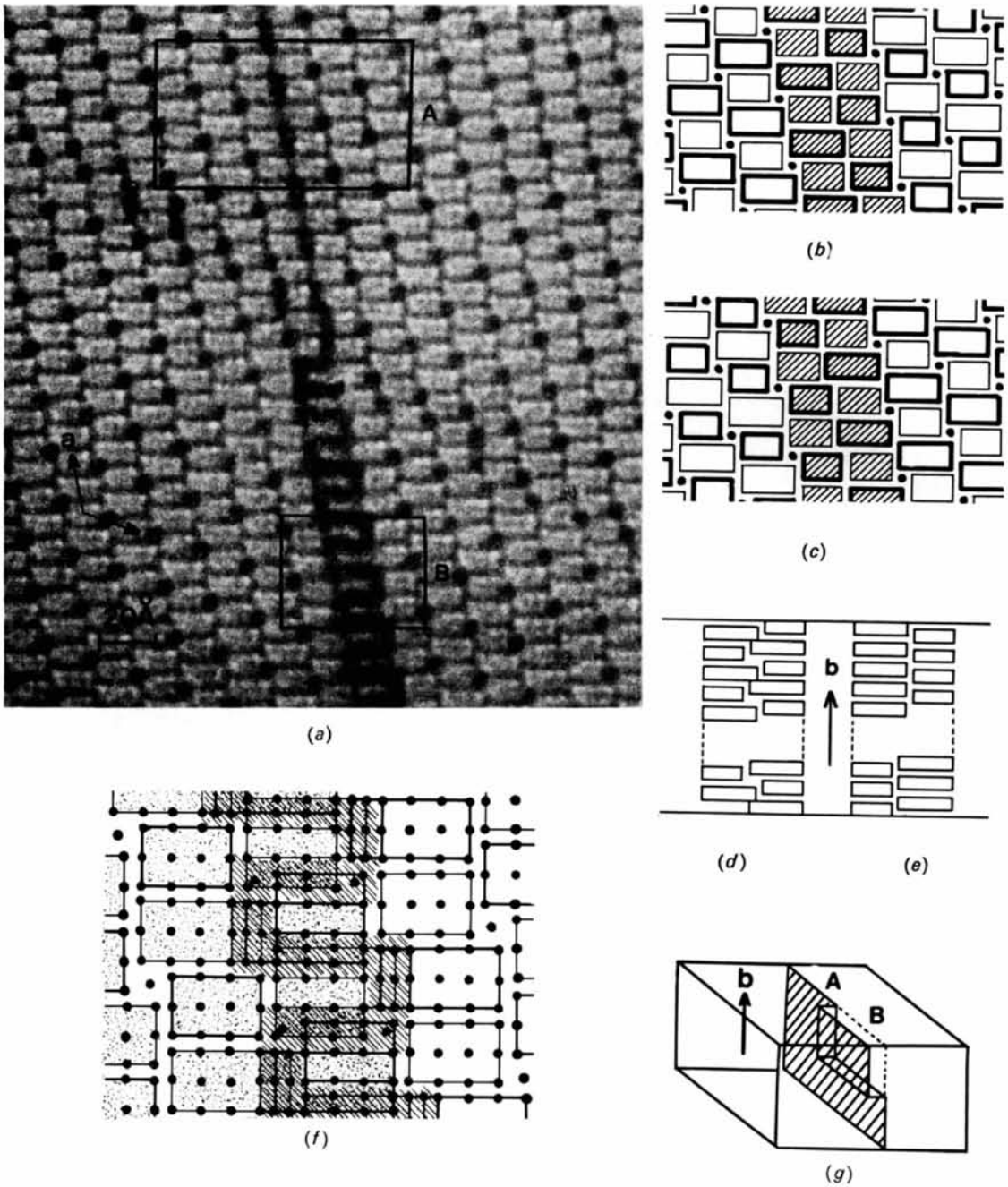

Fig. 11. (*a*) Two-dimensional lattice image showing another defect of type *D*, composed of two parts (shown by *A* and *B*). The contrast of *A* can be explained by a superposition of two different arrangements of the blocks along the *b* axis shown in (*b*) and (*c*). The model shown in (*d*) is a possible arrangement for the packing of the blocks along the *b* axis, preferred to that in (*e*). (*f*) Distribution of the metal-atom positions projected onto the *ac* plane in the defect corresponding to the area outlined by *B* in the image. Black dots represent metal atom positions in the projection. The three-dimensional defect plane which is displaced near the middle of the specimen thickness is illustrated in (*g*).

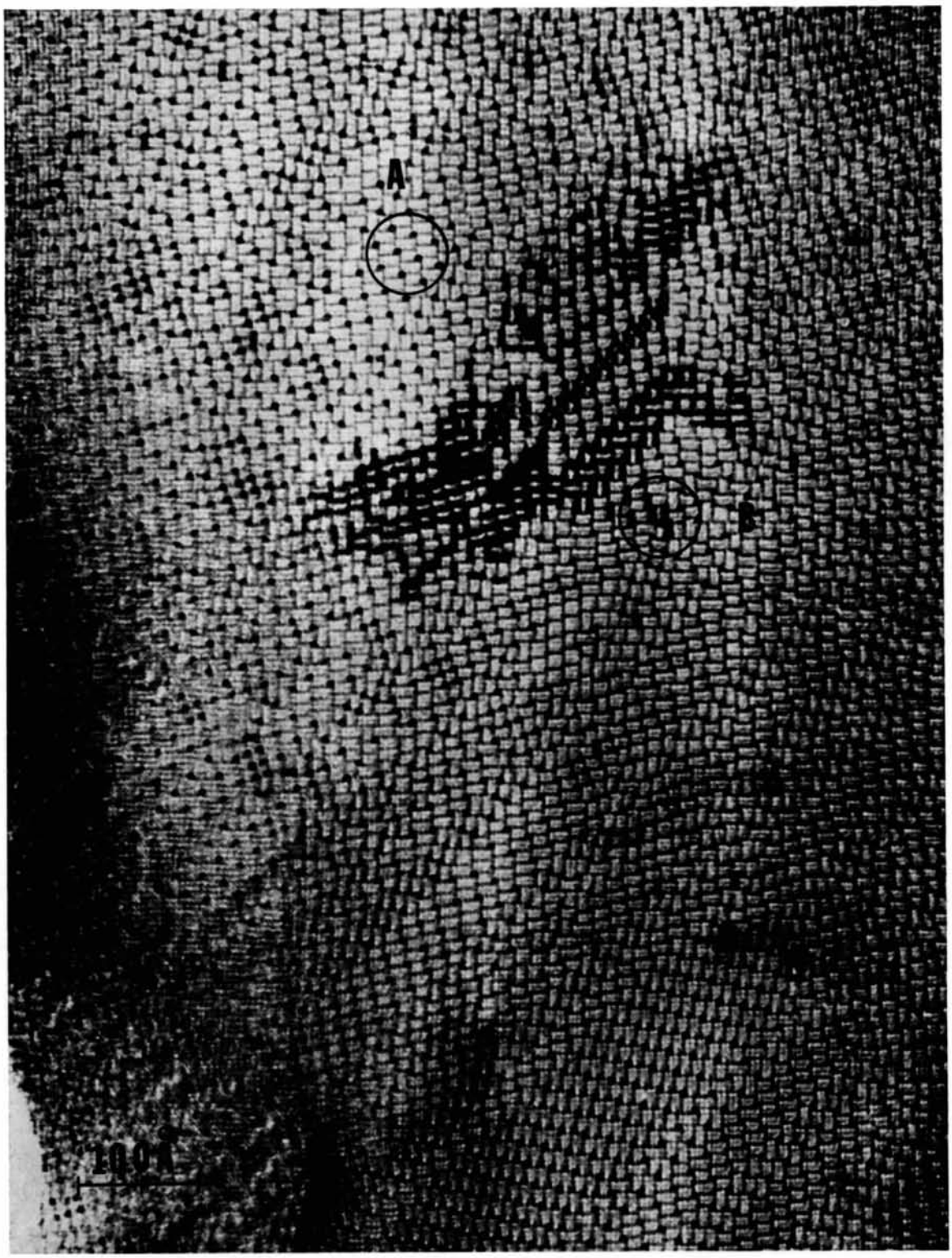

Fig. 12. Two-dimensional lattice image of a heavily disordered region of a crystal of H-Nb_2O_5 quenched from the melt. A locally ordered region (shown by *A*) and micro-twin bands at the bottom right are seen.

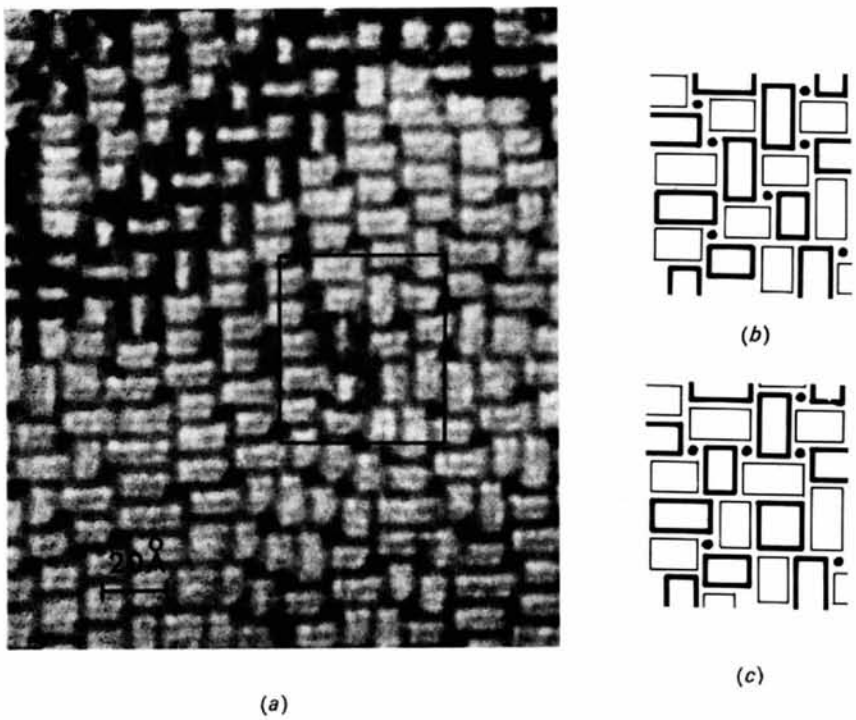

Fig. 13. (*a*) Enlarged two-dimensional lattice image of the area indicted by *B* in Fig. 12 showing abnormal black contrast, corresponding to the higher-density region of the metal-atom positions in the *ac*-plane projection, obtained by superposing the two different block arrangements shown in (*b*) and (*c*).

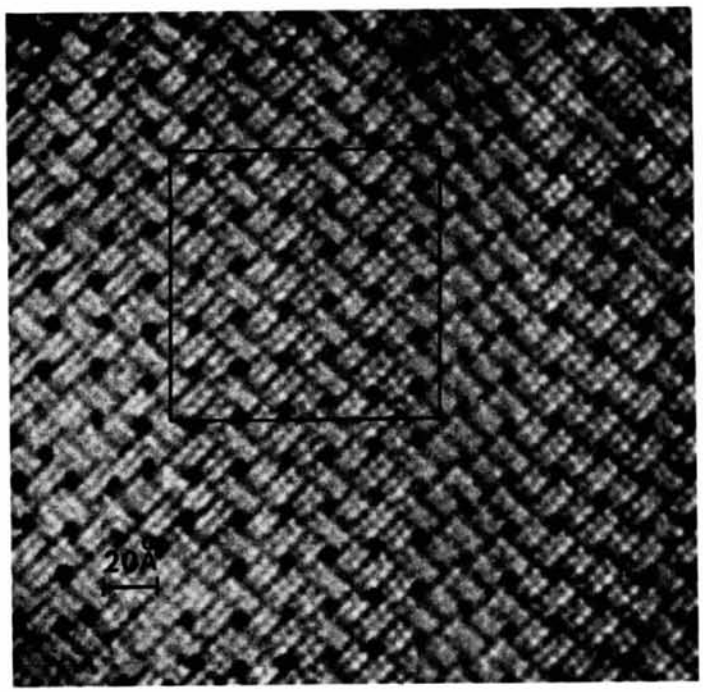

(a)

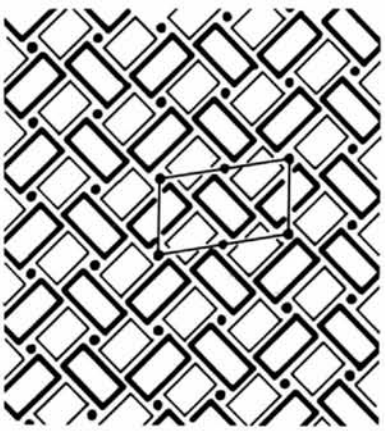

(b)

Fig. 14. (*a*) Two-dimensional lattice image showing a local ordering whose composition is Nb_2O_5 ($Nb_{56}O_{140}$) and (*b*) its model. The structure has the dimensions $a=19$, $b=3{\cdot}8$, $c=32$ Å and $\beta=80°$.

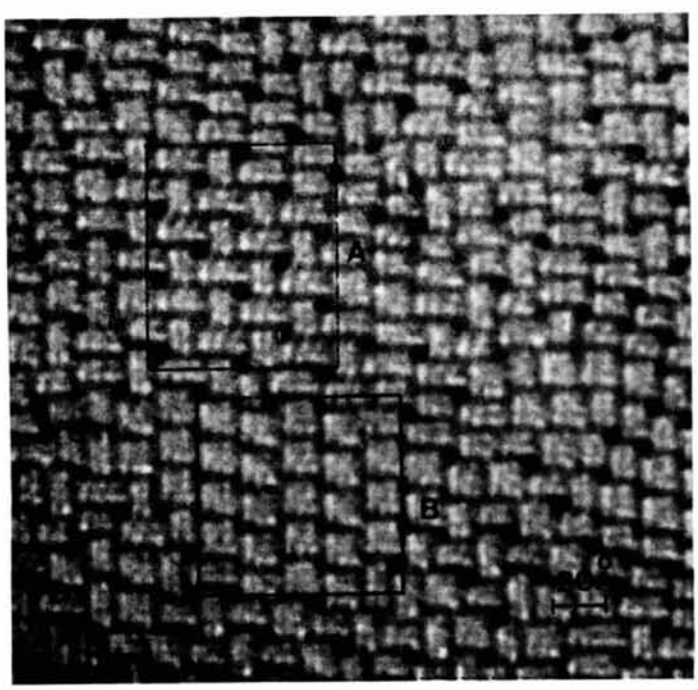

(a)

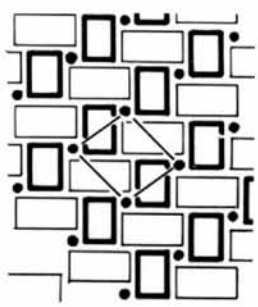

(b)

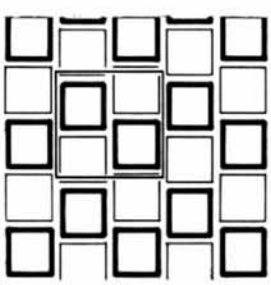

(c)

Fig. 15. (*a*) Two-dimensional lattice images showing other local ordering in a heavily disordered region, where two polymorphs of Nb_2O_5($Nb_{28}O_{70}$) (shown by *A*), and the orthorhombic structure of N-Nb_2O_5 composed of 4×4 blocks (shown by *B*), are seen. Their models are represented in (*b*) and (*c*).

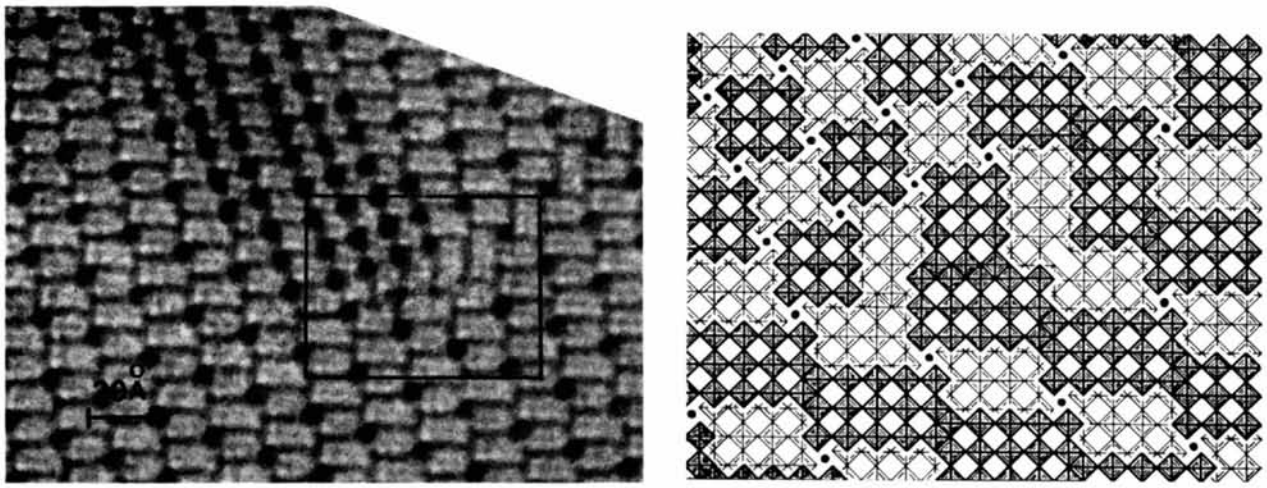

(*a*) (*b*)

Fig. 16. (*a*) Two-dimensional lattice image showing an irregular packing of the blocks at the intersection of two defects and (*b*) its octahedral model.

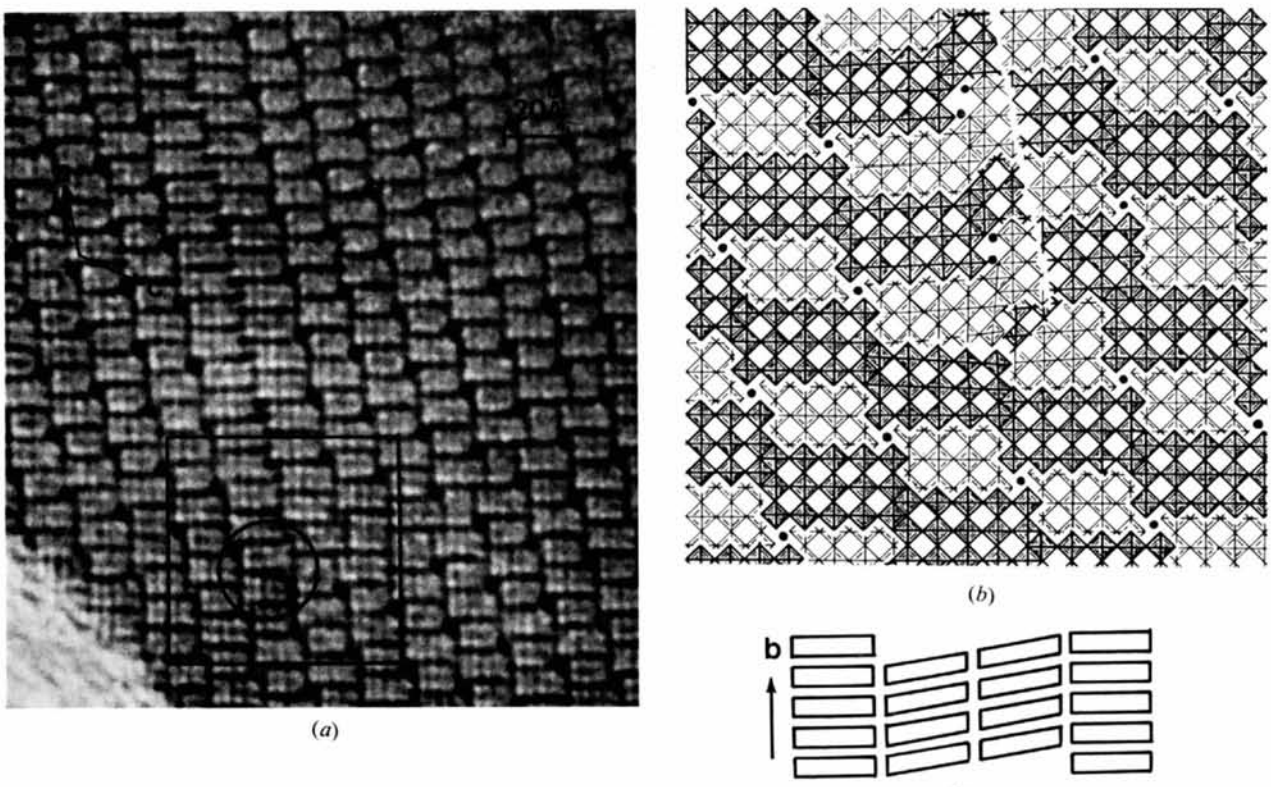

(*a*) (*b*) (*c*)

Fig. 17. (*a*) Two-dimensional lattice image showing incoherently packed blocks (enclosed by circle) at the terminal of the defects and (*b*) its octahedral model. The model shown in (*c*) is an arrangement for the packing of the blocks across the defect along the *b* axis.

[*To face p.* 25

each block in a number of photographs, but this is rather tedious. The defects of type B and C do not alter the composition but the defects of type A (intergrowth of the $WNb_{12}O_{33}$ type structure) and type D allow the crystal to have an oxygen excess. However, actually there is a local fluctuation of the composition near the intersections of the defect planes and the stoichiometry should be considered over a whole crystal, including heavily disordered regions, where the defects seem to be those which will maintain stoichiometry. Consequently it must be tentatively concluded that the present quenched crystal of H-Nb_2O_5 is hypo-stoichiometric*. In order to discuss the stoichiometry of this crystal in detail, it would be necessary to investigate the effects of annealing and to observe specimens containing no heavily disordered regions.

The diffusion mechanism in the binary compounds of Nb_2O_5 and other transition metal oxides has so far been speculated by comparison with various related phases of H-Nb_2O_5 (Andersson & Wadsley, 1969). Using high-resolution microscopy, useful information on this may be obtained by examining crystals of H-Nb_2O_5 with which has been mixed a very small amount of the other oxides or impurities and also it may be possible to observe directly solid state reaction at the level of atomic resolution under certain environments in the electron microscope.

It was found that twinning was a popular defect in these quenched specimens. The fact that the periodicity of the arrays of tetrahedral positions in multiple twin bands parallel to the b axis and the $\langle 101 \rangle$ directions was well retained, indicates that two-dimensional arrays of this type of ordering with a spacing of 15·4 Å are mainly dependent on the tetrahedrally coordinated niobium atoms.

Several new phases of Nb_2O_5 were revealed in defect structures and in a heavily disordered region. Regarding the PNb_9O_{25} type polymorph of Nb_2O_5 which was found in defect of type C, there is an ambiguity in that it could be regarded as the high temperature compound, $Ta_2O_5.2Nb_2O_5$ reported by Mohanty, Fiegel & Healy (1962) because a very small amount of Ta is contained in the Nb_2O_5 as an impurity and may be precipitated in the defect of type C during cooling.

The author wishes to thank Professor J. M. Cowley for his continuous encouragement and to Mr J. G. Allpress for providing samples and his critical reading of the manuscript and also to Professor M. O'Keeffe for his helpful suggestion. This work was supported by the National Science Foundation Area Development Grant in Solid State Science (No. GU3169).

* Recently J. G. Allpress has also made electron-microscopic observations on quenched H-Nb_2O_5 free from impurities and found that the defect of type A in his materials. He concluded that quenched materials of H-Nb_2O_5 are apparently non-stoichiometric (oxygen excess) and Wadsley defects (the defect of type A) must be accompanied by point defects of some kind, probably niobium interstitials or oxygen vacancies (Allpress, unpublished work).

References

ALLPRESS, J. G. & WADSLEY, A. D. (1969). *J. Solid State. Chem.* **1**, 28–38.
ALLPRESS, J. G., SANDERS, J. V. & WADSLEY, A. D. (1969). *Acta Cryst.* B**25**, 1156–1164.
ALLPRESS, J. G. (1970). *J. Solid State Chem.* **2**, 78–93.
ANDERSSON, S. (1967). *Z. anorg. allgem. Chem.* **351**, 106–112.
ANDERSSON, S. & WADSLEY, A. D. (1969). In *Perspectives in Inorganic Chemistry*, Vol. III. Edited by J. D. DUNITZ & J. A. IBERS. New York: John Wiley.
BRAUER, G. (1941). *Z. anorg. allgem. Chem.* **248**, 1–31.
COWLEY, J. M. & IIJIMA, S. (1972). *Z. Naturforsch.* **27a**, 445–451.
ERICKSON, H. P. & KLUG, A. (1970). *Ber. Bunsenges. Phys. Chem.* **74**, 1129–1137.
GATEHOUSE, B. M. & WADSLEY, A. D. (1965). *Acta Cryst.* **17**, 1545–1554.
GRINTON, G. R. & COWLEY, J. M. (1971). *Optik*, **34**, 221–233.
HEIDENREICH, R. D. & HAMMING, R. W. (1965). *Bell Syst. Tech. J.* **44**, 207–233.
IIJIMA, S. (1971). *J. Appl. Phys.* **42**, 5891–5893.
MOHANTY, G. P., FIEGEL, L. J. & HEALY, J. H. (1962). *Acta Cryst.* **15**, 1190.
ROTH, R. S. & WADSLEY, A. D. (1965). *Acta Cryst.* **19**, 26–32, 32–38, 38–42.
ROTH, R. S., WADSLEY, A. D. & ANDERSSON, S. (1965). *Acta Cryst.* **18**. 643–647.
SCHERZER, O. (1949). *J. Appl. Phys.* **20**, 20–29.
SHEASBY, J. S. & COX, B. (1968). *J. Less-Common Metals*, **15**, 129.
SPYRIDELIS, J., DELAVIGNETTE, P. & AMELINCKX, S. (1967). *Phys. Stat. Sol.* **19**, 683–704.